Self-Assembled Functional Molecular Materials for Optoelectronic Applications

Chi-Chung Kwok, Wei Lu and Chi-Ming Che*

Department of Chemistry and HKU-CAS Joint Laboratory on New Materials, The University of Hong Kong, Pokfulam Road, Hong Kong

ABSTRACT

There has been a growing interest to develop functional organic and organometallic materials in nano-scale by self assembly reactions as these materials could have unique electronic properties and applications. We have found that functionalized organometallic nano-wires which the formations are directed by weak Pt···Pt interactions along the dimension of the aggregates can be readily obtained by self-assembly reactions. These platinum(II) nano-wires exhibit interesting photophysical properties, vapochromic behavior, and could be used in the fabrication of organic (light-emitting) field-effect transistors.[1,2] We have also found that thermally stable coordination polymers (with decomposition temperature up to 490 °C), employing Zn^{2+} as template metal ion and Schiff base or terpyridine as repeating chelating units, could be easily synthesized by self-assembly reactions.[3,4] These zinc (II) coordination polymers exhibit intense blue to green photoluminescence, and their thin-film samples have PL quantum yields up to 0.55. Polymer light-emitting devices (PLEDs) employing these coordination polymers as emitters give blue and green EL with turn-on voltage as low as 5 V and maximum efficiency up to 2.0 cd A^{-1}.

INTRODUCTION

Metal-based quasi-one-dimensional structures derived from metallophilic Pt···Pt interactions, such as Magnus' green salt $[Pt(NH_3)_4]$ $[PtCl_4]$ [5] and Krogmann's salt $[K_2Pt(CN)_4Br_{0.3}](H_2O)_n$,[6] have long been known for decades. Overlapping between the $5dz^2$ orbitals of Pt(II) ions not only renders one-dimensional Pt(II) solids to have a deep color but also confers to them conducting[7] and sensing[8] properties. Recently, a microfilament of $[Pt(NH_2R)_4][PtCl_4]$ (R is an alkyl group) was made by electro-spinning and found to be a *p*-type semiconductor.[9] In literature, planar Pt(II) complexes with aryl α-diimine and/or cyclometalating ligands have been demonstrated to aggregate in solid state[10] or in non-polar solvents[11] through Pt···Pt and/or π–π interactions. In recent years, one-dimensional nanostructures of organic molecules[12] and metal complexes have been reported to have properties distinctly different from that of discrete molecules. We made one-dimensional nanostructures self-assembled from the heteroleptic binuclear Pt(II) complex {[(C^N^N)PtCl][(C^N^N) PtC≡O]}(PF_6) (**1**, HC^N^N = 6-(4'-methylphenyl)-2,2'-bipyridine). Solution-processible nanostructured films of this complex exhibited n-type semiconducting behavior in a bottom-contact TFT (thin-film field-effect transistor) configuration.

We envisage that it may be feasible to develop organic light-emitting field-effect transistors (OLEFETs) by incorporating switching and photoluminescent properties of platinum(II) nanostructures into a single compact device. We thus investigate the self-assembled organoplatinum(II) nanowires and their electroluminescent and ambipolar semiconducting

properties. Phosphorescent nanowires were self-assembled from cyclometalated/terpyridyl platinum(II) complexes bearing auxiliary arylisocyanide/arylacetylide ligands.

Polymers are widely regarded as promising materials for optoelectronic devices. Polymer light-emitting devices (PLEDs) generally give superior performance including low turn-on voltage, ease of fabrication and greater stability with no recrystallization problem as that encountered for small molecules in OLEDs.[13] However, the practical applications of many functional polymeric systems, in particular aryl π-conjugated polymers such as polyphenylene vinylene (PPV), poly(*p*-phenylene) (PPP), polythiophene (PT) and polyfluorene (PFO) in LED are limited by their intrinsic properties. For example, although PPV-based materials demonstrate high photoluminescence (PL) and electroluminescence (EL) efficiencies as well as color-turning properties, long-term stability of these EL devices is obstructed by photo-oxidative degradation.[14] For PPP, its relative insolubility poses a problem. While PT and related derivatives have been shown to display EL from blue to near infrared region, devices fabricated from these materials generally have low quantum efficiencies. PFO, a blue EL emitter, shows good thermal stability and high efficiency, but chain aggregation and ketone defect sites in the polymer can induce degradation of the EL devices.[15,16] We made a series of self-assembled metal coordination polymers which show color emission from violet to red with high PL quantum yields and good PLED efficiencies.

EXPERIMENTAL DETAILS

A mixture of **2** (19.0 mg, 0.04 mmol) and **3** (24.5 mg, 0.04 mmol) in CH_3CN (5 mL) was stirred for 10 min. The resulting red solution was filtered and evaporated to dryness to give a dark blue solid which was collected on a sinter-glass filter and washed thoroughly with CH_3OH, CH_2Cl_2 and Et_2O. Yield: 80%.

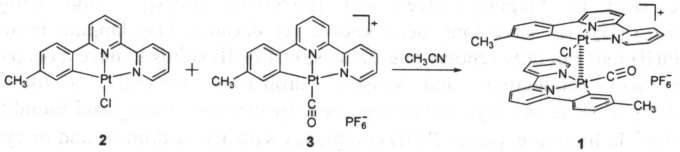

Scheme 1. Synthesis of the hybrid binuclear complex **1**.

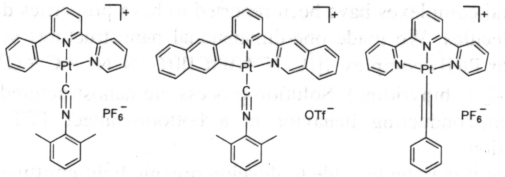

Scheme 2. Building blocks for self-assembled phosphorescent organoplatinum(II) nanowires.

Complexes **4** and **5** were prepared by a simple ligand substitution reaction of the corresponding cyclometalated platinum(II) chloride precursor with arylisocyanide. Complex **6**

was prepared according to the reported procedures. Precipitation method was adopted to prepare the nanowires. The complex was first dissolved in acetonitrile to give a bright yellow solution (*ca.* 1.0 mM, 100 μL). Nanowires were obtained as a purple, orange or green dispersion for **4** – **6**, respectively, by injecting acetonitrile solution into deionised water (1 mL). Nanowires were collected by centrifuge and re-dispersed in deionised water for three times.

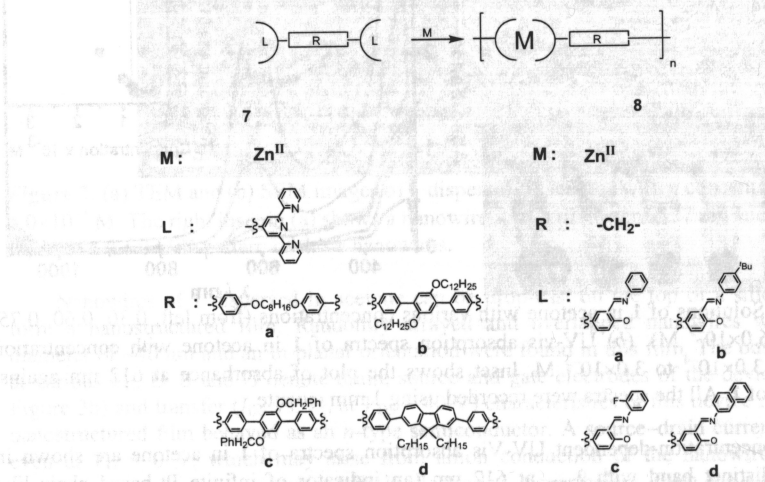

Scheme 3. Synthetic scheme for **7a** – **8d.**

The synthesis of zinc terpyridine polymers **7a** – **7d** are depicted in scheme 3. The synthesis of **7d** is described as an example. The other polymers were prepared in a similar manner. $Zn(OAc)_2{\cdot}2H_2O$ (0.1 mmol) in *N*-methylpyrrolidinone (NMP) (5 mL) was added dropwise to a NMP solution (50 mL) of terpyridine monomer (0.1 mmol). The resulting solution was heated at 105 °C under a nitrogen atmosphere for 24 hours. KPF_6 (1 mmol) was added into the hot solution. The resulting solution was poured into methanol (200 mL) and the precipitate obtained was purified by repeated precipitation using dimethylacetamide (DMAc) and methanol. The polymer was dried *in vacuo* at 80 °C for 24 hours and collected as a yellow solid. Yield: 80 %. The inherent viscosity of **7a** – **7d** ranges 0.62 to 1.21 dL g^{-1}, as determined using an Ubbelohde viscometer in NMP at 30±0.1 °C.

Synthesis of zinc Schiff base polymers **8a** – **8d** (Scheme 3). The synthesis of **8a** is described as an example. The other polymers were prepared in a similar manner. $Zn(OAc)_2{\cdot}2H_2O$ (0.1 mmol) in dimethylformamide (DMF, 5 mL) was added dropwise to a DMF solution (5 mL) of salicyladimine monomer (0.1 mmol). The mixture was heated at 100 °C under a nitrogen atmosphere for 24 hours. Upon cooling to room temperature, the resulting solution was poured into methanol (50 mL). The precipitate obtained was purified by repeated precipitation using DMF and methanol. The polymer was dried *in vacuo* at 80 °C for 24 hours. Yield: 79 %. The number-average molecular weight (M_n) for **8a** – **8d** ranges from 13580 to 19720, as determined using Gel Permeation Chromatography (GPC) with polystyrene as the standard in tetrahydrofuran (THF) at 35 °C.

DISCUSSION

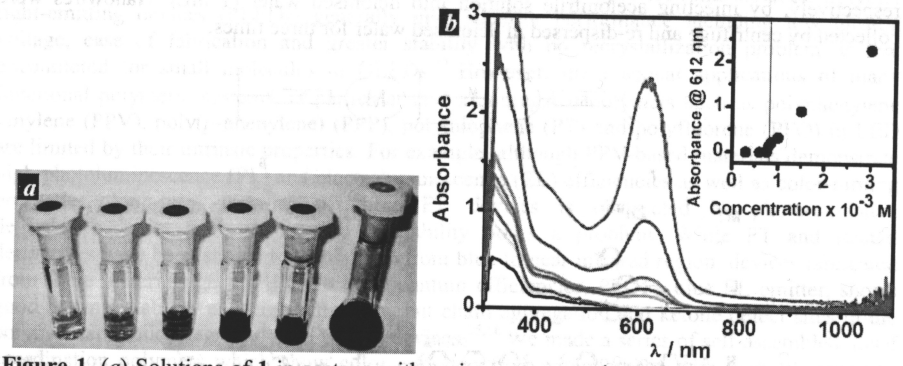

Figure 1. (*a*) Solutions of **1** in acetone with various concentrations (from left, 0.30, 0.60, 0.75, 1.5, 3.0 and 6.0×10^{-3} M). (*b*) UV-vis absorption spectra of **1** in acetone with concentration ranging from 3.0×10^{-4} to 3.0×10^{-3} M. Inset shows the plot of absorbance at 612 nm against concentration of **1**. All the spectra were recorded using 1 mm cuvette.

The concentration-dependent UV-Vis absorption spectra of **1** in acetone are shown in Figure 1. A distinct band with λ_{max} at 612 nm (an indicator of infinite Pt-based chain-like backbone) develops when the concentration of **1** is greater than 8.0×10^{-4} M. The blue color of the dispersion in acetone comes from nanowires with a uniform diameter of ~30 nm and length extending over 10 μm, as revealed by transmission electron microscopy (TEM) (Figure 2a) and scanning electron microscopy (SEM) (Figure 2b) images of the dispersion in acetone with a concentration of 6×10^{-3} M. Two *d*-spacings, 0.338 and 0.684 nm, structures were deduced from the electron diffraction rings in the selected area electron diffraction (SAED) pattern (Figure 2a, inset). It is noteworthy that the complexes **2** and **3** alone did not form blue-colored nanowires under the same conditions. These nanowires can be further dispersed into cyclohexane, toluene, Et_2O, MeO^{t}Bu or water. TEM and SEM images of these dispersions revealed nanorods with a uniform diameter of ~30 nm and lengths spanning over 300 nm. Thus dilution and sonication can shorten the length of nanowires but do not affect the diameter.

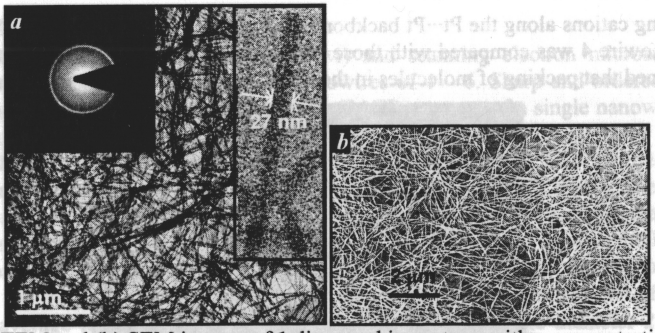

Figure 2. (a) TEM and (b) SEM images of **1** dispersed in acetone with a concentration of 6.0×10^{-3} M. The right inset in (a) shows a nanowire with a diameter of 27 nm and the left inset in (a) shows the SAED pattern of these nanowires.

Nanowires of **1** dispersed in acetone can be drop-cast on the top of a silicon substrate to form a nanostructured film. Randomly arrayed and overlapped nanowires with an average diameter of ~40 nm and an in-planar orientation were found in this film. The output (I_{DS} vs. V_{DS} at various V_G, D, S and G denote drain, source and gate electrodes of the device, respectively, Figure 3b) and transfer (I_{DS} vs. V_G at V_{DS} = 40 V) characteristics of this device revealed that the nanostructured film behaved as an *n*-type semiconductor. A source–drain current was observed even at V_G = 0 V, which may arise from anion conduction of the nanowires and the bulk conduction between the source and drain electrodes. Nevertheless, from the output curves, the field-effect electron mobility (μ_e) at the saturation regime was calculated up to 10^{-2} $cm^2V^{-1}s^{-1}$. Thus **1** belongs to the few examples of transition metal complex-based semiconductors for TFT applications.

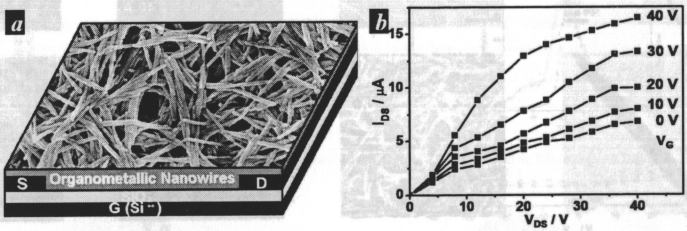

Figure 3. (a) SEM image of the surface of a bottom-contact TFT device with nanostructured **1** as semiconductor. (b) Output (I_{DS} vs. V_{DS}) characteristics of this TFT device.

The crystal structure of a needle-like crystal of **4**·H_2O was determined by crystallography. The salient feature of the crystal structure of **4**·H_2O is the Pt···Pt chain along the *c*-axis with alternative intermetal separations of 3.382(2) and 3.344(2) Å (Figure 4). These Pt···Pt distances are shorter than the sum of van der Waal's radii (3.44 Å), indicating extended d^8···d^8 interactions in the solid state. The cyclometalated platinum(II) moiety and the arylisocyanide ligand are co-planar, and this cationic plane is roughly perpendicular to the *c*-axis. There are two alternative C(isocyanide)–Pt–Pt–C(isocyanide) torsion angles (111.8° and 180.0°) between two

neighbouring cations along the Pt···Pt backbone. The powder X-ray diffraction (XRD) of a dried film of nanowire **4** was compared with those patterns simulated using the crystal data of **4**·H_2O and confirmed that packing of molecules in the nanowires resembled that in crystal **4**·H_2O.

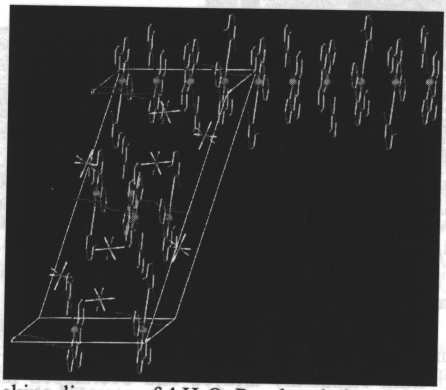

Figure 4. Crystal packing diagram of **4**·H_2O. Purple: platinum; blue: nitrogen; gray: carbon; yellow: fluorine; orange: phosphorus; red: oxygen.

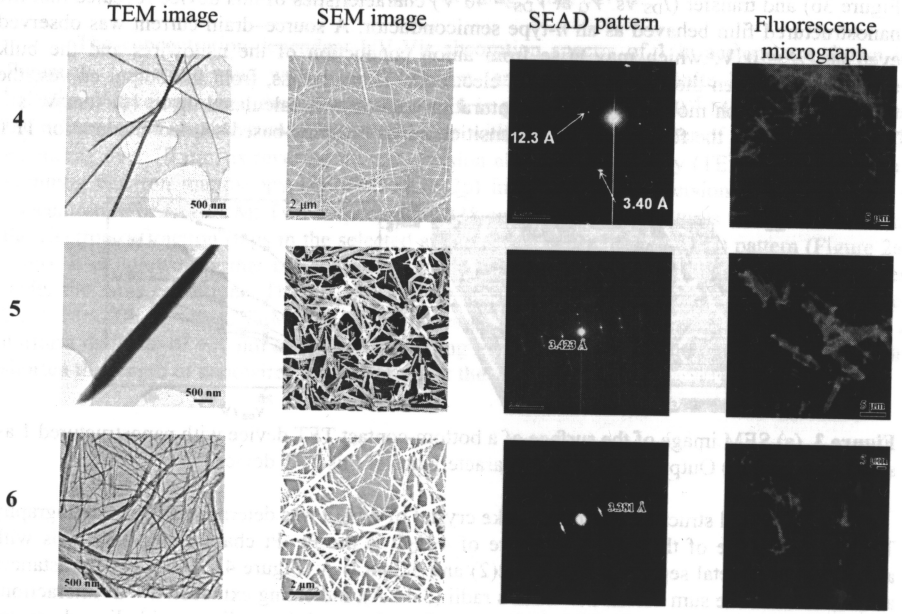

Figure 5. TEM image, SAED pattern, SEM image and Fluorescence micrograph (upon excitation at 550 nm) of the nanowires prepared with **4** – **6**.

Transmission electron microscopy (TEM) and scanning electron microscopy (SEM) images confirmed the pseudo-1-D nature of nanowires of **4** – **6**. Sharp and ordered spots were observed in the selected area electron diffraction (SAED) pattern of a single nanowire of **4** – **6**. The *d*-spacings along the long axis of nanowires of **4**, **5** and **6** are 3.40, 3.46 and 3.38 Å respectively. Based on the X-ray and electron diffraction data, the growth direction of the nanowires coincides with the *c*-axis, that is, along the long axis of Pt···Pt chains. We suggest that Pt···Pt interaction directs the anisotropic growth of these nanowires. The average diameter of the nanowires was 25±3 nm with a monodispersity of 12.4%. For nanowires of **4**, the length of the nanowires spanned from 2.0 to 3.5 μm with an average value of 2.2 μm. Submicron wires of **5** prepared with the same procedure as **4** were found to have much larger diameter of 253±54 nm and a longer average length of 3.8 μm. Nanowires **6** have an average diameter 27±4 nm and length of 1.0–1.5 μm.

Nanowires **4** - **6** showed intense red to near infrared (NIR) emission at λ_{max} 668, 607 and 742 nm, respectively. The saturated-red emission from segregated nanowires of **4** was directly observed under a fluorescence microscope with an excitation wavelength of 550 nm. Furthermore, typical phenomenon of optical waveguide was revealed for submicron wire of **5**, indicating that the wires of **5** are able to absorb excitation light and propagate the light-emission towards the tips. Upon laser excitation at 488 nm and viewed under a confocal laser scanning microscope (CLSM), submicron wire of **5** exhibited an orange emission with bright spots at both ends of the wire and a weaker emission observed from the wire body. The spatially resolved 3-D image of the edge emission from a single submicron wire of **5** showed two distinct peaks at both ends of the wire.

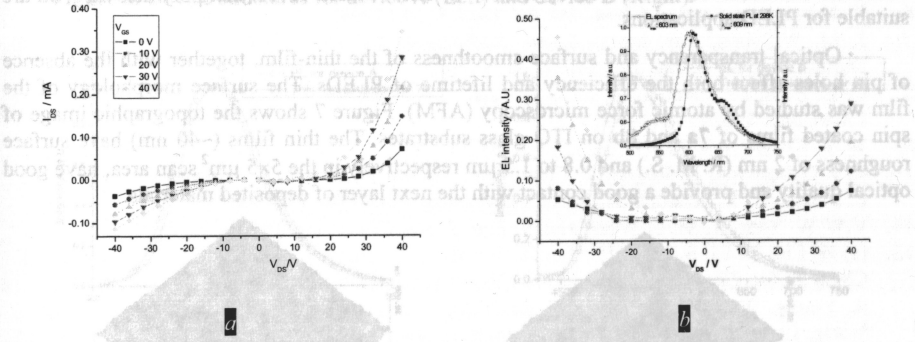

Figure 6. (a) Output characteristics (I_{DS} vs. V_{DS}) and (b) electroluminescence intensity (I) of OLEFET device made up of nanowires **5** after annealing at 350 K. (inset) EL and solid state PL spectra at 298K for **5**.

Studies on the semiconducting and electroluminescent properties of these self-assembled nanowires were conducted by using bottom contact FET configuration. Aqueous dispersions of

nanowires **4**, **5** and **6** were drop-cast on the top of patterned SiO_2 substrates. Figure 6 shows the output characteristics (I_{DS} versus V_{GS} at different V_{DS}) as well as electroluminescence intensity from the bottom contact OLEFET device with nanowires of **5** as active layer after annealing at 350 K. Ambipolar behaviour was observed, as indicated by the fact that the drain source current I_{DS} increased with increasing both positive and negative gate voltage. The field effect was found to be affected by the annealing temperature. Increases in current intensity and up to 1000-fold enhancement of field effect mobility were found for the annealed film when compared to the non-annealing one. The highest mobility was achieved at an annealing temperature of 350 K. This remarkable enhancement in mobility is consistent with the formation of larger crystal domains observed upon annealing the latter is anticipated to decrease the crystal grain boundary. We found that nanowires/submicron wires of **4**, **5** and **6** behave as ambipolar semiconductors with both hole and electron mobility around 10^{-1} $cm^2V^{-1}s^{-1}$.

Upon a positive or negative gate bias, electroluminescence was observed from the OLEFET devices. The intensity of the light emission from these devices increased with increasing gate voltages (Figure 6b). Electroluminescent spectrum from the OLEFET device with nanowires of **5** as active material is depicted in Figure 6b (inset). The electroluminescence peak maximum is at 603 nm which is comparable in energy to the corresponding photoluminescence (λ_{em} = 609 nm for solid state PL **5**).

As the metal cathode of polymer light-emitting devices (PLEDs) is fabricated by thermal deposition, materials used in PLEDs must possess a good thermal stability to stand for this fabrication process. The thermal stability of **7a** – **8d** was studied by thermogravimetric analysis (TGA). The decomposition temperature (T_d) is up to 461 °C (**8d**). Recrystallization is one of the major factors affecting the lifetime of PLEDs, the material used must stay in amorphous state throughout the device fabrication process and during operation. The glass transition temperature (T_g) of the polymers were determined by differential scanning calorimetry (DSC), no phase transition was observed for **7a** – **8d** up to 300 °C. These results reveal that polymers **7a** – **8d** are suitable for PLED applications.

Optical transparency and surface smoothness of the thin-film, together with the absence of pin holes affect both the efficiency and lifetime of PLEDs. The surface morphology of the film was studied by atomic force microscopy (AFM). Figure 7 shows the topographic image of spin coated films of **7a** and **8b** on ITO glass substrates. The thin films (~40 nm) have surface roughness of 2 nm (R. M. S.) and 0.8 to 1.5 μm respectively in the 5×5 μm^2 scan area, have good optical quality and provide a good contact with the next layer of deposited materials.

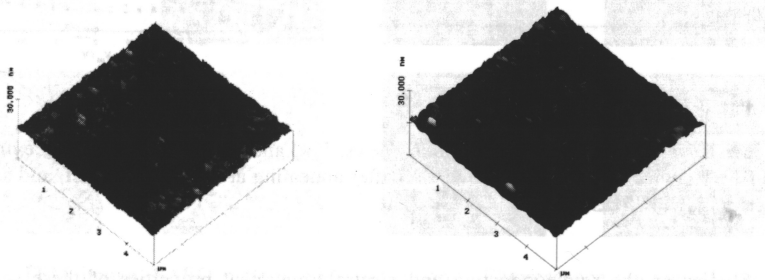

Figure 7. AFM (topographic) images of spin coated films of **7a** (left) and **8b** (right) on ITO glass.

The solution emission λ_{max} of **7a** – **8d** in DMF solutions are in the 450 to 518 nm range, which correspond to blue to green emission. The quantum yield ranges from 0.06 (**7a**) to 0.77 (**7b**). Polymer **7a** was fabricated into device **A** with configuration of ITO / poly(3,4-ethylenedioxythiophene):poly(styrenesulfonic acid) (PEDOT:PSS, 30 nm) / polymer (30–50 nm) / Ca (10 nm) / Al (100 nm), while **8b** was fabricated into device **B** with configuration of ITO / PEDOT : PSS (30 nm) / polymer (30–50 nm) / 2,9-dimethyl-4,7-diphenyl-1,10-phenanthroline (BCP, 20 nm) / tris(8-hydroxyquinolino)-aluminum (Alq, 20 nm) / LiF (0.5 nm) / Al (200 nm). Both the EL spectra of devices **A** and **B** are similar to the PL of the corresponding spin-coated polymer films, revealing that the same excited state could be responsible for both EL and PL emissions.

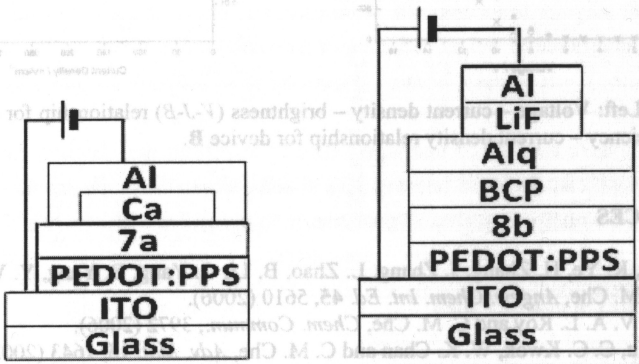

Figure 8. Device structures for device **A** (Left) and device **B** (Right).

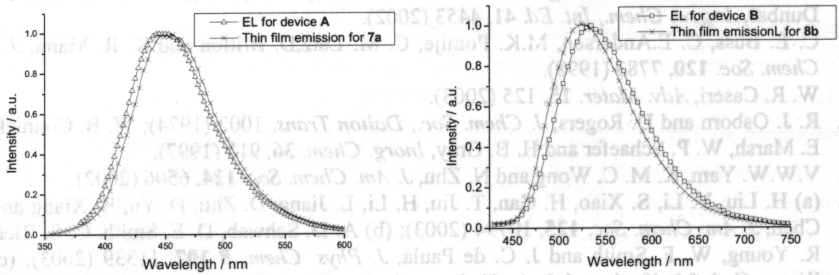

Figure 9. Comparisons of EL spectra of devices **A** and **B** with the corresponding polymers.

Device **A** has a turn-on voltage of 6 V, and the maximum efficiency of the device is 0.8 cd A^{-1}. The maximum luminance of 1700 cd m^{-2} was obtained at a driving voltage of 13 V. The CIE_1931 coordinates of device **A** are x = 0.15, y = 0.21. Device **B** has a turn-on of 5 V, and the maximum efficiency of the device is 2.0 cd A^{-1} at 8 V. The maximum luminance of 3120 cd m^{-2}

was obtained at 15 V. Device **B** showed a green emission with λ_{max} at 536 nm and CIE_1931 coordinates of x = 0.30 and y = 0.55.

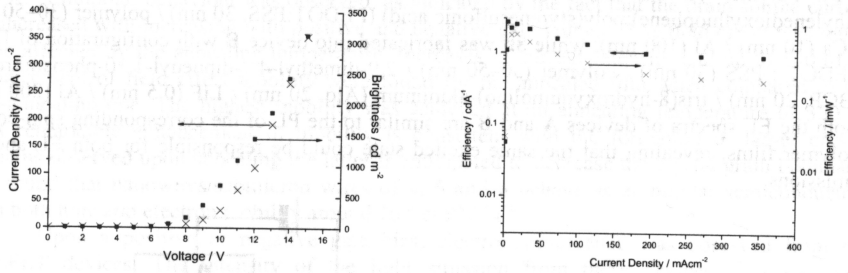

Figure 10. Left: Voltage – current density – brightness (*V-J-B*) relationship for device **B**. Right: Device efficiency – current density relationship for device **B**.

REFERENCES

1. Y. Sun, K. Ye, H. Zhang, J. Zhang, L. Zhao, B. Li, G. Yang, B. Yang, Y. Wang, S.-W. Lai and C. M. Che, *Angew. Chem. Int. Ed.* **45**, 5610 (2006).
2. W. Lu, V. A. L. Roy and C. M. Che, *Chem. Commun.*, 3972 (2006).
3. S. C. Yu, C. C. Kwok, W. K. Chan and C. M. Che, *Adv. Mat.* **15**, 1643 (2003).
4. C. C. Kwok, S. C. Yu, I. H. T. Sham and C. M. Che, *Chem. Commum.* 2758 (2004).
5. G. Magnus, *Ann. Chim. Phys.* **40**, 110 (1829).
6. K. Krogmann, Angew. *Chem., Int. Ed. Engl.* **8**, 35 (1969).
7. J. M. Williams, *Adv. Inorg. Chem. Radiochem.* **26**, 235 (1983); J. K. Bera and K. R. Dunbar, *Angew. Chem., Int. Ed.* **41**, 4453 (2002).
8. C. E. Buss, C. E.Anderson, M.K. Pomije, C. M. Lutz,D. Britton and K. R. Mann, *J. Am. Chem. Soc.* **120**, 7783 (1998).
9. W. R. Caseri, *Adv. Mater.* **15**, 125 (2003).
10. R. J. Osborn and D. Rogers, *J. Chem. Soc., Dalton Trans.* 1002 (1974); W. B. Connick, R. E. Marsh, W. P. Schaefer and H. B. Gray, *Inorg. Chem.* **36**, 913 (1997).
11. V.W.W. Yam, K. M. C. Wong and N. Zhu, *J. Am. Chem. Soc.* **124**, 6506 (2002).
12. (a) H. Liu, Y. Li, S. Xiao, H. Gan, T. Jiu, H. Li, L. Jiang, D. Zhu, D. Yu, B. Xiang and Y. Chen, *J. Am. Chem. Soc.* **125**, 10794 (2003); (b) A. D. Schwab, D. E. Smith, C. S. Rich, E. R. Young, W. F. Smith and J. C. de Paula, *J. Phys. Chem. B* **107**, 11339 (2003); (c) Z. Wang, C. J. Medforth and J. A. Shelnutt, *J. Am. Chem. Soc.* **126**, 15954 (2004); (d) M. Morikawa, M. Yoshihara, T. Endo and N. Kimizuka, *J. Am. Chem. Soc.* **127**, 1358 (2005).
13. (a) L. Akcelrud, *Prog. Polym. Sci.* **28**, 875 (2003). (b) U. Mitschke, and P. Bauerle, *J. Mater. Chem.* **10**, 1471 (2000), (c) A. Kraft, A. C. Grimsdale and A. B. Holmes, *Angew. Chem. Int. Ed.* **37**, *402* (1998).
14. J. C. Scott, J. H. Kaufman, P. J. Brock, R. DiPietro, J. Salem and J. A. Goitia, *J. Appl. Phys.* **79**, 2745 (1996).
15. U. Scherf and E. J. W. List, *Adv. Mater.* **14**, 477 (2002).

16. (a) C. Xia and R. C. Advincula, *Marcomolecules* **34**, 5854 (2001). (b) V. N. Bliznyyuk, S. A. Carter, J. C. Scott, G. Klarner, R. D. Miller and D. C. Miller, *Marcomolecules* **32**, 361 (1999). (c) F. Klarner, J. I. Lee, V. Y. Lee, E. Chan, J. P. Chen, A. Nelson, D. Markiewicz, R. Siemens, J. C. Scott and R. D. Miller, *Chem. Mater.* **11**, 1800 (1999).
17. M. Y. Yuen, V. A. L. Roy, W. Lu, S. C. F. Kui, G. S. M. Tong, M. H. So, S. S. Y. Chui, M. Muccini, J. Q. Ning, S. J. Xu and C. M. Che, *Angew. Chem., Int. Ed.* **120**, 10043 (2008).